

Article

High-Order Harmonics Generation in Selenium-Containing Plasmas

Rashid A. Ganeev ^{1,2,3,4}

¹ Laboratory of Nonlinear Optics, Institute of Astronomy, University of Latvia, Jelgavas iela 3, LV-1004 Riga, Latvia; rashid.ganeev@lu.lv

² Institute of Fundamental and Applied Research, TIAME National Research University, Kori Niyazov Street 39, Tashkent 100000, Uzbekistan

³ Department of Physics and Chemistry, Chirchik State Pedagogical University, 104 Amir Temur, Chirchik 111700, Uzbekistan

⁴ Department of Physics, Voronezh State University, 394006 Voronezh, Russia

Abstract: The studies of the high-order harmonics generated in Se-containing plasmas are reported. The ablation of selenium in a vacuum allowed for the formation of a plasma demonstrating high-order harmonics generation and resonance enhancement of the harmonic at the shortest wavelength reported so far ($\lambda \approx 22.9$ nm, $E_{ph} \approx 54.14$ eV). This harmonic corresponds to the 35th order of the 800-nm-class lasers. The influence of the presence of selenium in the molecular state (ZnSe and HgSe) on the suppression of the resonance effect during harmonics generation in plasma is studied. The enhanced 35th harmonic was analyzed by different methods of plasma formation using nanosecond, picosecond, and femtosecond pulses. The enhancement factor of the resonance-enhanced harmonic was measured to be $32\times$ compared with the neighboring lower-order harmonics in the case of the picosecond-pulses-induced Se plasma. The role of the strong ionic transition of Se in the region of 22.7 nm in the observation of the resonance-induced enhancement of a single harmonic is discussed.

Keywords: selenium-containing plasma; high-order harmonics generation



Citation: Ganeev, R.A. High-Order Harmonics Generation in Selenium-Containing Plasmas. *Photonics* **2023**, *10*, 854. <https://doi.org/10.3390/photonics10070854>

Received: 26 June 2023
Revised: 18 July 2023
Accepted: 22 July 2023
Published: 24 July 2023



Copyright: © 2023 by the author. Licensee MDPI, Basel, Switzerland. This article is an open access article distributed under the terms and conditions of the Creative Commons Attribution (CC BY) license (<https://creativecommons.org/licenses/by/4.0/>).

1. Introduction

A few metal-based laser-induced plasmas (LIPs) such as atomic Ag, In, Mn, Cr, and Au have demonstrated attractive properties as the media for high-order harmonics generation (HHG) allowing the observation of the strong plateau-like harmonic spectra in the extreme ultraviolet (XUV) region [1–12]. Some of these LIPs demonstrate the resonance-induced enhancement of a single harmonic. Contrary to that, the molecular structures comprising those atoms notably modify the ability in the resonance-induced enhancement of harmonics and decrease the HHG conversion efficiency, leading to the generation of weaker and featureless plateau-like harmonic spectra. This process was demonstrated in the case of the chromium-containing LIP when the application of the molecular structure caused a notable decrease in or complete disappearance of the resonance-induced enhancement of a single harmonic [13]. A similar feature was reported in the case when the two-color pump (TCP) of LIP was used for HHG instead of the single-color pump (SCP) [14].

To analyze the processes leading to the restrictions in observation of the resonance harmonic (RH) effect, one has to choose a plasma medium demonstrating the enhancement of single harmonic up to the shortest wavelength range. In that case, two limiting factors (molecular-versus-atomic LIP and TCP-versus-SCP) can be precisely distinguished. So far, the highest generating orders enhanced due to the RH effect were reported in the case of Cr (29th order of 800-nm-class lasers, H29), Mn (H31), and Se (H35) LIPs. In this context, two former plasma media were analyzed in a few previous publications [13,15–18]. In the meantime, the selenium-containing plasma has rarely been used as a medium for harmonics generation [17,19]. Additionally, the HHG studies on this and other atomic

plasmas were predominantly carried out using 800-nm-class Ti sapphire lasers. No reports about resonance harmonic generation were published in the case of the Se-containing molecular LIPs or in the case of the application of longer-wavelength lasers for HHG in Se plasma. Additionally, no influence of laser ablation conditions using pulses of different duration on the harmonic spectra from the Se LIP was analyzed so far, to the best of our knowledge.

In this paper, we analyze various abovementioned features during application of the atomic and molecular Se species for HHG using the variable conditions of plasma formation. Se-containing plasmas comprising atoms and molecular structures were compared with each other from the point of view of the harmonic yield, spectral distribution of harmonics, and generation of RH. The conditions of the maximal yield of the RH (35th harmonic of 800 nm pump) compared with other harmonics from Se LIP were determined.

2. HHG in Selenium-Containing Plasmas

The standard approach for the analysis of the influence of plasma characteristics on the HHG in LIP [20] was applied in this study. The left panel of Figure 1 shows a scheme of the experimental setup for HHG comprising the target-containing vacuum chamber and the XUV spectrometer. The femtosecond driving pulses were focused inside the LIP. The plasma was produced by the heating pulses of different duration. We used a pure selenium target to analyze the conditions of the plasmas produced by the pulses of different duration. The molecular targets (ZnSe and HgSe) were also analyzed to compare with the HHG in the atomic (Se) LIP.

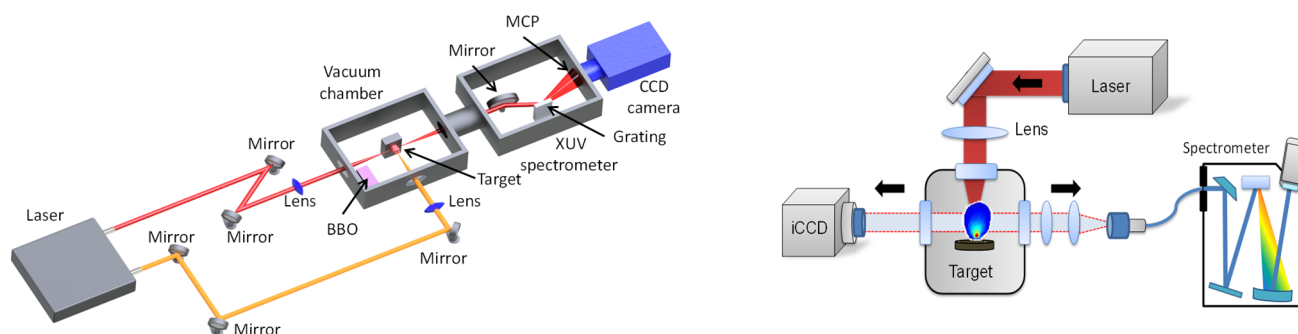


Figure 1. (Left) panel: scheme for HHG in plasma. The path of picosecond heating pulses is shown in yellow. The path of femtosecond driving pulses is shown in red. MCP: microchannel plate. (Right) panel: scheme for the analysis of plasma characteristics. iCCD: intensified charge-coupled camera. The red color and arrow show the direction of the heating pulses towards the target. The left arrow shows the direction of the observation for the collection of the plasma image by a iCCD camera at different moments from the beginning of target ablation. The right arrow shows the direction of the observation of plasma emission for the analysis of the spectrum of LIP.

To determine the characteristics of Se-containing LIP, laser-induced breakdown spectroscopy and time-resolved analysis of plasma spreading were used. The scheme for the analysis of the plasma characteristics is shown in the right panel of Figure 1. A selenium target ($2 \times 2 \times 1 \text{ mm}^3$ plate) was used for plasma formation. The density of plasma varied depending on the distance between the target and the optical axis of propagation of the driving pulses, as well as on the pulse duration of the heating pulses. Correspondingly, the efficiency of harmonics generation became a function of the delay between the heating and driving pulses. Overall, the optimized delay between heating and driving pulses and the optimized heating pulse fluence became the key parameters ensuring efficient HHG in Se-containing plasmas.

Figure 2a shows a raw image of plasma spreading out from the selenium target at an 80 ns delay from the beginning of ablation by picosecond pulses. This optimal delay between heating and driving pulses during HHG experiments with Se-containing LIPs

was established by calculation of the velocity of the plasma cloud, which allowed for matching the arrival of the driving pulses in the area above target surface with the time when the highest concentration of particles was achieved at a distance of 0.3 mm from the ablation spot. The optimal delay was also defined empirically by determining the maximal harmonic yield of the Se LIP. The plasma spectrum in the visible and UV ranges is shown in Figure 2b.

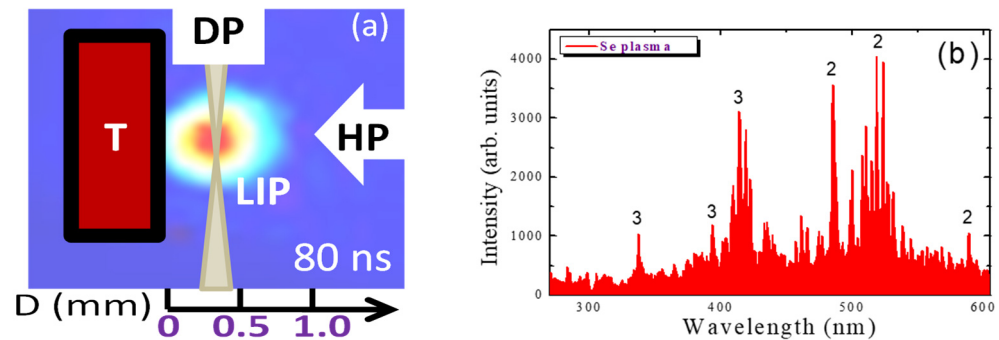


Figure 2. (a) Raw image of the plasma spreading out from the Se target at an 80 ns delay from the beginning of ablation. T: target; DP: driving pulse; HP: heating pulse; LIP: laser-induced plasma. Bottom line shows the distance (D) from the target surface. The driving beam propagated 0.3 mm above the target surface. (b) UV-visible spectrum of Se plasma in the case of ablation by picosecond pulses. The numbers on the spectral curve correspond to the ionization states of transitions.

The time-dependent analysis of plasma spreading at different moments from ablation allows for defining the optimal delay between the heating pulse producing plasma and the driving pulse propagating through this plasma by determining a velocity of the central part of plasma cloud. Here, the term “optimal delay” refers to the conditions of plasma formation and spreading at which the maximal yield of harmonics can be achieved. To determine these conditions one has to allow plasma to spread out of the surface such that the density of particles becomes maximal during propagation of the driving pulses at a distance of 0.3 mm above the target. This is a distinct requirement for the interaction of the driving radiation with the largest available number of plasma particles. Since the harmonic yield quadratically depends on the concentration of plasma, one can assume that before and after the optimal delay between heating and driving pulses the number of emitting coherent XUV photons will be decreased.

We analyzed plasma dynamics using different images of plasma at variable delays between pulses. In Figure 2a, we show one of them corresponding to the moment of the propagation of the driving beam through the densest component of LIP. The brightest spots of plasma at a distance of 0.3 mm from the target surface were observed at the delays between 70 and 100 ns. Further spreading of plasma at a longer delay caused a decrease in its concentration along the path of the femtosecond driving pulses.

Figure 2b shows the UV-visible spectrum of Se plasma at the conditions when the highest harmonic yield was achieved alongside the strong H35, i.e., at a 7 J cm^{-2} fluence of the heating picosecond pulses. One can see that this plasma was overheated in terms of the optimal conditions commonly used during HHG in LIPs. This spectrum shows the ionic lines of doubly and triply ionized selenium. The concentration of plasma at these conditions was maximal from the point of view of the phase-mismatch-induced limitation of further growth of the fluence of the heating pulse. These conditions of plasma formation allowed generation of strong harmonics and observation of the extended harmonic cutoff. Moreover, the excited doubly and, probably, triply charged ions allowed for the creation of the conditions for the resonance enhancement of the 35th harmonic of the 800 nm laser. The appearance of the transitions attributed to the doubly and triply charged ions in the visible and UV ranges may indicate the presence of similar transitions in the analyzed region of

XUV. Meanwhile, our further studies of Se plasma emission in the short-wavelength range showed that the XUV emission does not appear in the 10–40 spectral range.

The comparison of the emission spectra of Se and ZnSe plasmas showed that, under similar conditions of ablation, the latter species spread at lower velocity. The luminescence spectra were almost similar, while some ionic transitions of Zn and some uncharacterized lines appeared in the case of the molecular plasma. Our further studies showed that over-excitation of ZnSe and HgSe caused a decrease in HHG conversion efficiency, probably due to larger amount of free electrons in plasma area compared to the case of Se plasma. It is hard to judge from the plasma emission about the optimal conditions for observation of the 35th harmonic enhancement. The plasma emission in the visible and UV ranges is just an additional indicator which can point out the conditions when the doubly and triply charged transitions in the XUV range may play important role in the enhancement of a single harmonic.

Two laser sources were used for HHG in the studied plasmas. A Ti sapphire laser produced the 800 nm, 65 fs, 10 Hz pulses, which were used for the SCP of Se LIP. Another laser source provided the tunable 70 fs pulses in the near-infrared (NIR, 1200–1600 nm) spectral range. The intensity of driving pulses inside the LIP in both cases was maintained at $3.5 \times 10^{14} \text{ W cm}^{-2}$ to allow the comparative studies of harmonic yield using the driving pulses of different wavelengths. Some HHG experiments were carried out using the TCP of Se LIP. A 0.3 mm thick barium borate (BBO) crystal was installed inside the target chamber on the path of focused pulses to allow for generating the second harmonic emission, which then participated in HHG alongside the driving 800 nm and NIR pulses. The conversion efficiencies of the second harmonic pulses were 5% and 7% in the cases of 800 nm and 1400 nm driving pulses, respectively.

The picosecond heating pulses (800 nm, 250 ps) for HHG were obtained by separating part of the uncompressed laser radiation before the compressor of the Ti sapphire laser. The intensity of the pulses on the target surface varied between 2.3×10^{10} and $1.3 \times 10^{11} \text{ W cm}^{-2}$.

The first sets of harmonic generation studies were carried out using the Se-containing plasmas comprising the ablated molecular structures (zinc selenide and mercury selenide). In the case of 800 nm driving pulses, the application of these ablated molecular Se-containing LIPs did not reveal the generation of RH in the region of 22.9 nm, which was reported in an earlier study of HHG in the case of ablation of the atomic Se target [17]. In the case of HgSe LIP, the plateau-like harmonics up to the 43rd harmonic were observed (H43, Figure 3a). H35 ($\lambda = 22.9 \text{ nm}$) was not enhanced compared with H33. A similar feature was observed in the case of the harmonics generated in ZnSe plasma (Figure 3b). H35 was barely seen in this harmonic spectrum.

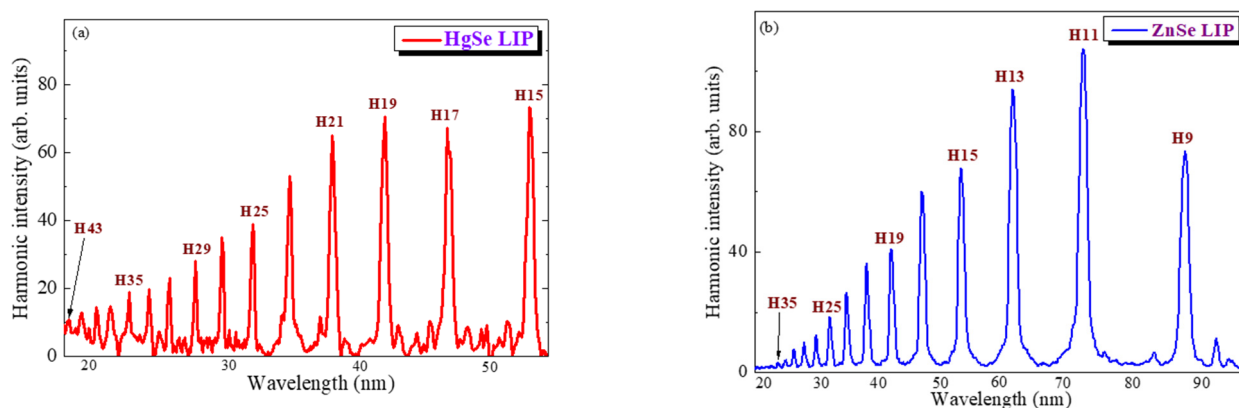


Figure 3. HHG in the Se-containing quantum dot and molecular plasmas. (a) Harmonic spectrum in the case of HgSe LIP. (b) Harmonic spectrum in the case of ZnSe LIP.

To achieve the resonance enhancement of a single harmonic in Se-containing plasma, one has to use the ablation of the target containing only Se atoms. Another requirement is the optimization of the laser ablation of the Se bulk target. This term refers to the formation of a plasma dominantly comprised of neutral, singly, and doubly charged Se, alongside a small concentration of free electrons. The latter particles notably decrease the phase-matching conditions in the case of HHG in LIPs. The process of deterioration of the phase-matching conditions between the interacting waves of driving and harmonic emission strongly depends on the pulse duration of the heating pulses. Additionally, the phase mismatch between these waves becomes emphasized in the shorter-wavelength region of harmonic spectra.

To determine the most suitable conditions for the ablation of the selenium target, we used heating pulses of different duration. The ablation by nanosecond pulses was accomplished using a Nd YAG laser providing 10 ns pulses. This laser was synchronized with the driving femtosecond laser to allow for defining the best delay between the heating and driving pulses (70–90 ns in the case of the driving beam propagating at a distance of 0.3 mm above the surface of the ablating target). The ablation by picosecond pulses (250 ps) was carried out using the same methods which were applied for the studies of HHG in HgSe and ZnSe plasmas. The application of femtosecond pulses for laser ablation was performed by dividing the compressed 65 fs beam into two beams. The first beam was used for the laser ablation, while the second beam propagated through the optical delay line to maintain the 80 ns delay between two (heating and driving) femtosecond pulses in the plasma area. We determined the conditions of maximal harmonic yield in each case of ablation by pulses of different duration. The same intensity of the driving pulses ($3.5 \times 10^{14} \text{ W cm}^{-2}$) was maintained during these experiments.

Figure 4 shows the generated spectra using the 800 nm pump in the vicinity of the harmonic cutoffs in the case of three LIPs produced by (a) 10 ns, (b) 250 ps, and (c) 65 fs heating pulses at approximately similar fluence of the heating pulses on the target surface (2.5 J cm^{-2}). In the former case, only a weak 19th harmonic (H19) was observed in the 17–44 nm spectral range (Figure 4a). The low value of harmonic cutoff obtained in that case can be explained by the presence of a high concentration of free electrons during the relatively long process of target ablation, thus restricting the phase-matching conditions for the highest orders of harmonics.

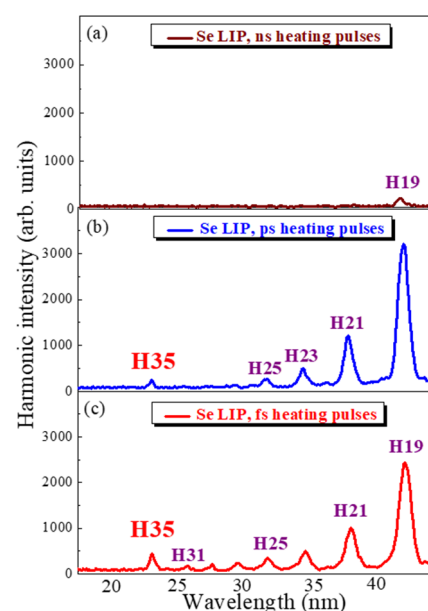


Figure 4. Highest-order harmonic spectra from the plasma produced in the selenium bulk target using the (a) nanosecond, (b) picosecond, and (c) femtosecond heating pulses.

The application of shorter pulses (250 ps and 65 fs) allowed for diminishing the effect of the presence of free electrons in the plasmas by decreasing their concentration at the used fluence of heating pulses. In the case of picosecond heating pulses, the harmonic cutoff was extended up to H25 (Figure 4b). The most important feature, in that case, was the unusual appearance of RH (H35), which was not surrounded by the neighboring harmonics. This observation of the enhanced single harmonic, which was not observed in the case of HgSe and ZnSe LIPs, nor in the case of the Se LIP produced by nanosecond pulses, points out the achievement of the plasma conditions at which the ionic transitions in the vicinity of 22.9 nm ($E_{ph} = 54.14$ eV) possess large oscillator strength (gf). Notice that the intensity of H35 was approximately equal to the one of H25 in the case of the picosecond heating pulses.

An approximately similar RH was observed in the case of the formation of Se LIP using femtosecond pulses (Figure 4c). One can see the enhanced H35 that appeared after very weak H33. The extension of the cutoff compared to the case of picosecond pulses-induced plasma was attributed to the smaller concentration of the free electrons produced by the 65 fs pulses at the optimal conditions of HHG. Notice the absence of the higher-order harmonics above RH (H35).

The application of nanosecond pulses for laser ablation of the Se bulk target allowed for the analysis of HHG in a long-time scale from the beginning of ablation. Previously, the appearance of nanoparticles during the ablation of bulk selenium by 10 ns pulses was reported in [21]. It was found that the size, shape, and population of selenium nanoparticles strongly depended on the experimental conditions during the ablation process, in particular, on the fluence of laser pulses. The broad range of the sizes of nanoparticles assumes that those multi-particle species spread out from the surface at different velocities. Correspondingly, one can expect their appearance on the path of the driving femtosecond pulses at different moments from the beginning of ablation.

Initially, the atomic species reach the area of driving pulses propagation (~ 0.3 mm above the target surface), and then the small aggregates (clusters) and large structures (quantum dots and nanoparticles of different sizes) appear on the path of a driving laser beam. Figure 5a shows the dependence of the intensity of the 17th harmonic generating in Se LIP on the delay between the heating (10 ns) and driving (65 fs) pulses. The range of delay variations was 0–10⁵ ns. It was observed that H17 generated up to the 7 μ s delay between pulses. These measurements showed that the plasma consisted of atoms/ions and clusters of different sizes. The latter species have masses from a few times to a few ten thousand times larger than the single-atomic particles. Correspondingly, the velocities of these clusters, especially those possessing large masses, were significantly lower than the velocities of the atoms and ions presented in LIP. Those heavy particles arrived in the area of interaction with driving pulses much later than the atoms and ions. Their appearance and interaction with femtosecond pulses caused the generation of harmonics, though not as strongly as in the case of single-atomic species. The harmonic yield from atoms and ions was expectedly higher due to the larger concentration of these species compared with the heavy clusters and nanoparticles. Earlier, a similar conclusion was reported in the case of the generation of the lower-order harmonics in nanosecond-pulses-induced LIP [22].

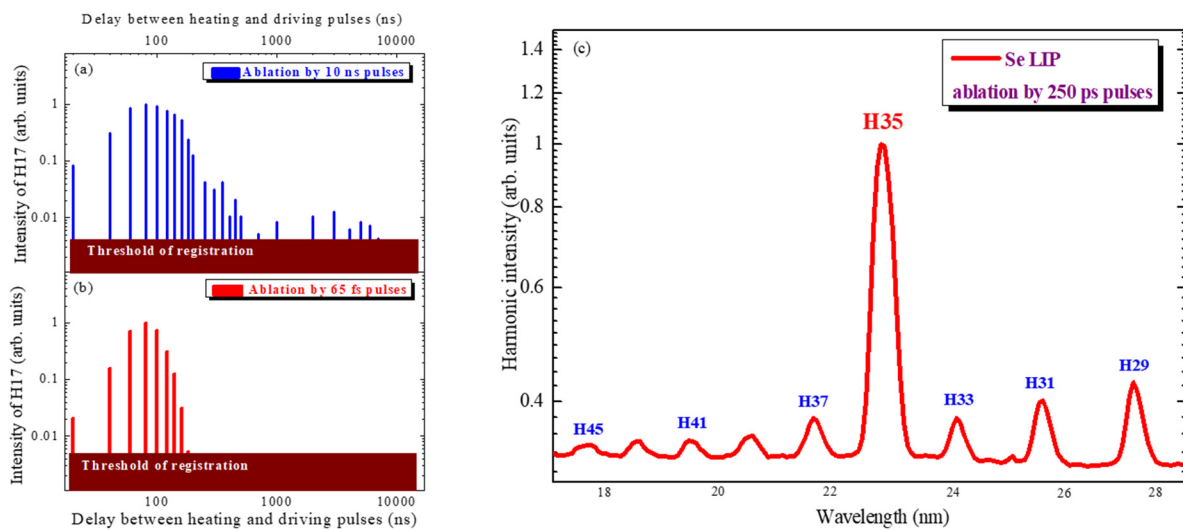


Figure 5. Dependencies of the H17 yield from the Se plasma on the delay between heating and driving pulses in the case of (a) ablation by nanosecond pulses and (b) ablation by femtosecond pulses. (c) Harmonic spectrum from Se LIP in the case of the optimal ablation using 250 ps pulses at the fluence of 7 J cm^{-2} .

We did not observe the harmonics generation during large delays in the case of ablation of the Se target by shorter pulses. Particularly, the maximal yield of the same 17th harmonic generating in femtosecond-pulses-induced plasma was achieved in the range of 60–80 ns, similar to the case of 10 ns pulses, and then was significantly decreased at larger delays. No high-order harmonics were observed at the delays exceeding 300 ns (Figure 5b). The same feature was observed in the case of the ablation of the Se target by 250 ps pulses. These observations point out the absence of a sufficient amount of multi-particle aggregates during ablation using short laser pulses at the conditions when the fluence of heating pulses satisfies the requirement of generation of the strongest harmonic yield.

Our studies showed the advantages of the application of shorter heating pulses for the formation of the optimal selenium plasma and for the demonstration of the RH effect, allowing observation of the enhanced harmonic. Our following studies allowed for determining the best conditions for the ablation of Se bulk target, which revealed that the maximal harmonic yield, harmonic cutoff, and RH effect can be achieved using picosecond heating pulses. Below, we show that the growth of the concentration of ions causes the influence of the ionic transition responsible for the resonance enhancement of H35 on the whole pattern of the harmonic spectrum, despite the growing concentration of free electrons.

Figure 5c shows the harmonic spectrum from the Se LIP in the case of the optimal ablation using 250 ps pulses at a fluence of 7 J cm^{-2} . This spectrum is significantly distinguished from the one shown in Figure 4b and obtained at a fluence of heating pulse of 2.5 J cm^{-2} . Apart from notably enhanced H35, the cutoff was significantly extended (up to H53). The resonantly enhanced harmonic was stronger than any harmonic in the studied spectral range (17–28 nm). The H35:H33 ratio of harmonic intensities was ~ 32 . The RH was approximately equal to H15 (not shown in this graph). Meanwhile, the application of TCP (800 nm + 400 nm) and the generation of odd and even harmonics in the case of Se LIP under similar conditions of plasma formation did not allow for observation of the RH effect in the vicinity of the 22.9 nm wavelength. The maximal harmonic order achieved in that case was H23 ($\lambda = 34.8 \text{ nm}$). Though the lower-order even harmonics were notably stronger than the odd harmonics, a significant decrease in harmonic cutoff did not allow the generation of H35 using the TCP of Se LIP.

HHG was also optimized in the case of the longer-wavelength driving NIR pulses, similar to the 800 nm case. The change in pump wavelength led to variation in the phase matching between the interacting waves and, as a consequence, affected the conditions for

optimal ablation of the Se target. Notice that the application of the single-color pulses of NIR radiation (1310 and 1420 nm) did not allow the generation of high-order harmonics in spite of the $E_h \propto \lambda^2$ rule of the three-step model [23]. Here, E_h is the energy of the generating photons in the cut-off region and λ is a wavelength of driving pulses. The influence of the intensity of harmonics follows the $I \propto \lambda^{-5}$ rule [24], thus notably decreasing the HHG conversion efficiency, which did not allow for observing the higher orders of harmonics. Because of this, the application of the two-color pump (1310 + 655 nm and 1420 + 710 nm) was used, which allowed for the generation of harmonics up to the thirties orders (~ 40 nm). The attempts to further optimize plasma conditions for similar lengths of laser plasma (~ 0.5 mm) on the target surface did not lead to the enhancement of harmonics from these two-color pump schemes. Correspondingly, HHG was not observed in the region of single harmonic enhancement (~ 23 nm). Probably, the option could be an enhancement of the plasma length, which can amend the harmonic yield under better phase matching conditions for the NIR + H2 pump compared to the 800 nm pump. However, even under these conditions, no significant improvement of harmonic cutoff for the NIR + H2 pump was observed.

Figure 6 shows three comparative spectra of harmonics generated using the 800 nm, 1420 nm + 710 nm, and 1310 nm + 655 nm driving pulses in the case of the formation of Se LIP by picosecond pulses under similar conditions of ablation. In the former case (800 nm, upper panel), the H35 was comparable with the H17, while no neighbor harmonics appeared in this spectrum. These conditions of plasma formation did not repeat the conditions at which the maximal RH and cutoff were observed (Figure 5c), though the intensity of RH was again much stronger than that of the neighboring harmonics. Notice that the formation of Se LIP in this set of experiments corresponded to the best conditions of HHG using the NIR TCP pulses.

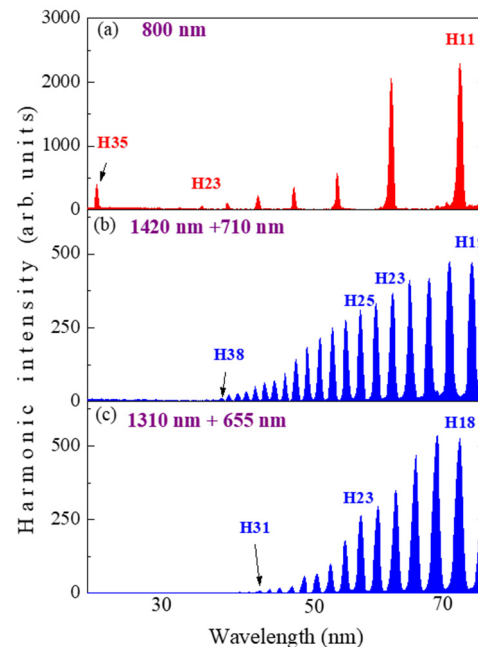


Figure 6. The comparative spectra of harmonics generated using the (a) 800 nm, (b) 1420 nm + 710 nm, and (c) 1310 nm + 655 nm driving pulses in the case of the formation of Se LIP by picosecond pulses. The measurements were carried out at an equal collection time.

The application of TCP using NIR pulses of different wavelengths (two bottom panels of Figure 6) allowed for the generation of the plateau-like shape of harmonics intensity distribution corresponding to the gradual decrease in the approximately equal odd and even harmonics. Their intensities were approximately five (in the case of 1420 nm + 710 nm pump) and four (in the case of 1310 nm + 655 nm pump) times lower than the intensities

of the harmonics produced by 800 nm pulses in the same spectral region (compare the intensity scales of the three harmonic spectra shown in Figure 6) at a similar intensity of the driving pulses and equal conditions of plasma formation. The difference in the harmonic efficiencies in the case of 800 nm and NIR pulses is attributed to the $I_h \propto \lambda^{-5}$ rule [24,25]. Notice that, in the case of NIR + H2 pumps, no harmonics appeared in the 22.9 nm region.

3. Discussion

The RH effect in the case of high-order harmonics generation in LIPs is an interesting and important topic. The first study of the harmonic spectrum from purely atomic Se plasmas in the 802 nm driving field [17] showed a strong resonance-induced 35th harmonic. Notice that those studies reported the observation of this effect in Se plasma without the (a) analysis of this process using heating pumps of different duration, (b) comparison with Se-containing molecular plasmas, (c) optimization of the delay between heating and driving pulses, or (d) application of longer-wavelength pulses for analysis of the RH effect. These processes were studied in the present paper, which allowed for achieving a significant enhancement of RH with regard to the neighboring harmonics (32×) compared with the referenced study (12×) [17].

Another previous study where selenium-containing species were analyzed used HgSe quantum dots [19]. A film containing HgSe QDs was ablated and the HHG using 1030 nm, 40 fs driving pulses was observed in the LIP containing the mercury sulfide quantum dots. High-order harmonics up to the 37th order were generated in the plasmas containing HgSe QDs. The wavelength of this harmonic (27.8 nm) was below the region where the RH effect could be observed (22.9 nm).

The resonance-enhanced effect during HHG in plasma is a rather complex process which can be described by the four-step model [26]. The first two steps are the same as in the three-step model, but instead of the last step (radiative recombination from the continuum to the ground state), the free electron is trapped by the parent ion so that the system (parent ion + electron) lands in the autoionizing state, and then it relaxes to the ground state emitting XUV. In addition, there are several theoretical studies in which the HHG efficiency was calculated using the recombination cross-section. The theoretical models other than the four-step model were introduced in [27–32], though the list of the theoretical studies of RH effect in plasma is much larger. A sequence of experiments on the pronounced enhancement of single harmonics in laser-driven plasmas has shown that this effect is attributed to the dynamical shift of ionic resonances close to specific harmonics. An overview of the studies of resonance processes in LIPs is presented in [33,34].

The demonstration of the resonance enhancement of single harmonics in different metal plasmas is currently useful from the point of view of the analysis of the spectral properties of those plasmas in the XUV range. Particularly, the demonstration of the enhancement of 35th harmonic in Se plasma was not predicted through the calculations of the high values of the oscillator strength of ionic transitions in the 22.9 nm region, contrary to some other plasmas (Cr and In). Thus, at the present stage of research, the application of the resonance-harmonic-induced processes is limited by a determination of the ionic transitions of metals possessing large gfs .

Below, we address the role of the collision and relaxation processes that may affect the concentration and temperature of Se plasma. In the present case, those processes were not taken into account. In the case of 10 ns heating pulses, the dynamics of H17 (Figure 5a), as well as any other harmonic, are driven by the presence of a sufficient amount of particles in the area of the optical axis of femtosecond pulses propagation. Those particles can be either atoms, ions, some aggregates comprising tens of particles, or even large agglomerates such as quantum dots and nanoparticles. The ablation of targets by long pulses may produce nanoparticles, which move at much lower speeds than the single-atomic species. Correspondingly, the slowly moving large species of plasma arrive in the area of interaction with femtosecond pulses at significantly longer delays. The harmonics at these conditions were observed while shifting the delay generator towards the range of a few microseconds

(Figure 5a). In the case of picosecond and femtosecond heating pulses, this scenario does not work.

Figure 5a,b show the dependencies of the H17 yield on the time delay between the two laser pulses by using different methods. This harmonic was chosen randomly. The same delay-dependent features as in the case of H17 were observed in the case of other harmonics. Particularly, H11 to H25 showed similar intensity-versus-delay dependencies. As mentioned, we did not observe harmonics generation at large delays in the case of ablation of the Se target by shorter pulses. The example of intensity-versus-delay is shown only for the 65 fs heating pulses (Figure 5b). Almost similar dependence was observed in the case of the 250 ps heating pulses. The time delay between heating and driving pulses in the case of the graph shown in Figure 5c corresponds to the conditions when the highest yield and cutoff extension of harmonics were achieved (80 ns).

A decrease or even disappearance of the resonant peak in the molecular plasma compared with the atomic one containing the ions responsible for the RH effect has been reported in a few studies. The physical mechanisms showing a distinction of the RH effect in atoms and molecules were discussed in [35]. In [36], this difference was analyzed in the case of atomic (Mo) and molecular (MoS₂) molybdenum-containing plasmas. The resonant harmonic generation from Mo-containing materials is due to the influence of 4p-4d resonant transitions from the single and double-ionized Mo [37]. The suppression of harmonics at 33–34 eV (~21H of 800 nm driving pulses) in laser-induced plasmas of MoS₂ was attributed to the contribution from the destructive interference of 4p-4d transitions with 4d orbital recombination [38]. The behavior of resonant transitions with recombined orbitals is important in HHG because macroscopically its yield depends on the interference of high-order harmonics generated from every ionic and atomic source. A similar feature may be responsible for the suppression of RH (H35) in ZnSe and HgSe plasmas. The experimental results show that the plasmas from the ZnSe and HgSe targets produce a less intense resonant harmonic, which indicates that those molecular ions affect the favorable conditions of resonance-induced enhancement of a single harmonic.

A difference in the extension of harmonic cutoffs in the case of these two molecular plasmas (H43 and H35 in the cases of HgSe and ZnSe, respectively) depends on various factors (band gap, conditions of plasma formation, intensity of the driving pulses, etc.). Zinc selenide has a large band gap ($E_g = 2.67$ eV). Meanwhile, mercury selenide exhibited a semi-metallic property with a negligible direct band gap of about 0 eV. It is hard to compare these two molecules, taking into account the three-step HHG formula under similar conditions of plasma formation.

ZnSe shows a rather abrupt, plateau-like shape of harmonics distribution (Figure 3b). The meaning of “plateau-like” distribution of the intensities of harmonics refers to the conditions when the drop of next harmonic order with regard to the preceding one does not follow the drop of harmonics intensity described by the perturbation theory. The perturbation theory predicts a decrease in each next harmonic by a factor of five or more. This rule is observed in the case of the lowest-order harmonics generation (i.e., from the 3rd to the 9th harmonic). Meanwhile, in the case shown in Figure 3b, the harmonics from H11 to H31 dropped only by one order of magnitude, which means the decay of each next harmonic with a factor of ~1.2 occurs like it should, taking into account the three-step model. The plateau does not mean that the harmonics remain similar to the order higher than H9. They also decrease, and in some cases notably so. However, by any means, the drop of harmonic efficiency in the case of the HHG described by the non-perturbative theory of light-matter interaction does not follow the abrupt drop described by the perturbative theory.

HHG in molecular plasmas containing oxides, phosphides, and selenides shows reduced or non-resonant harmonics [35]. One can assume that, apart from the above-mentioned destructive interference mechanism, the detuning/shifting of the resonant transition reduces the *gf* of this transition. Hence, the decreased resonant harmonic yield in the studied case might be due to the modification of the resonant transitions influenced

by Hg and Zn components, which may diminish the gf of the transition, thus leading to decay in the enhancement of single harmonic.

Below, we discuss why the resonance peak (H35) does not appear in the molecular target (ZnSe and HgSe plasma). The presence of Se-containing molecular components in the plasma may either detune or shift the resonant harmonic transition attributed to the Se ions. This modification may lead to a reduction in the gf of this transition followed by the generation of a featureless harmonic distribution like those shown in Figure 3. The detuning or shifting of the transition may occur due to the alternation of the refractive index of plasma at the resonant wavelength, which can lead to the modification in the phases of the interacting waves (i.e., driving wave and 35H from different plasmas such as Se, HgSe, and ZnSe). Two former species may affect the electrical and optical properties of the Se energy structure by the creation of new energy levels, which might lead to the generation of high-order harmonic spectra without the resonance characteristics for XUV photons at 22.9 nm.

To the best of our knowledge, there are no reports on the gf values of the transitions of Se ions in the region of the enhancement of single harmonics ($\lambda = 22.9$ nm, $E_{ph} \approx 54.1$ eV). Previous studies of Se transitions in the short-wavelength range were carried out down to 90 nm (13.8 eV, [39–41]). The highest photon energy range studied so far in the case of Se plasma (18.0–31.0 eV, [42]) was also below the range of energies at which the RH was observed. Meanwhile, the strong third-order line that corresponded to 54.62 eV energy ($\lambda \approx 22.7$ nm) was reported in [42] without the elaboration of the origin of this transition. Probably, this transition, which is close to the wavelength of H35, can be responsible for the enhancement of 35th harmonic in the case of Se plasma.

Meanwhile, there are no reports on the direct observation of this transition. The studies of the plasma emission from the atomic Se at high fluencies of the heating pulses exceeding the fluencies providing the best conditions for observation of RH did not reveal the emission of any transition in the vicinity of the wavelength of this harmonic. Probably, they can exist as non-radiative transitions, which cannot be observed by the methods of laser-induced excitation. This does not mean that such transitions do not exist. They may have weak emission properties. The NIST tables do not provide any information about the existence of any transitions below 31 eV [43], which are far from the anticipated 54 eV ($\lambda = 22.9$ nm) transition. Further studies of the energetic structure of Se in the short-wavelength region are required.

The harmonic efficiency in Se LIP at heating pulse duration of 250 ps is investigated in both Figures 4b and 5c. Notice that the efficiencies of H35 and H25 are comparable in Figure 4b. In contrast, the efficiencies of H35 and H25 differ significantly in Figure 5c. Below, a difference in the selection of laser parameters for these two experiments is explained. The results presented in Figure 4 comprise the application of the pulses of different duration for the formation of the laser-induced plasma. During experiments, approximately the same fluence of heating pulses on the target surface was maintained. The fluence of 250 ps pulses in these studies was not optimal for the generation of extended harmonics and the demonstration of the “optimal” RH effect when the enhancement of H35 was the highest among other conditions of experiments. Thus, the “non-optimal” fluence of the 250 ps pulses allowed a demonstration of the similarity of the RH and a relatively high (25th) harmonic. These experiments show that the RH effect was not as impressive as one can expect.

Then, with the optimization of the fluence of 250 ps pulses (actually, it was increased by almost three times, from 2.5 to 7 J cm⁻², compared with the case shown in Figure 4b), a significantly larger difference in the intensities of the RH and all neighboring harmonics was achieved (Figure 5c). At those “optimal” conditions of plasma formation, the RH considerably exceeded the 25th one. Actually, it became equal to H15. One of the most important features of RH is a distinction of its intensity with regard to the lowest possible order of generating harmonics, which allows its separation from other emissions using thin metal foils for practical applications. Notice that the intensity of the driving pulses was

similar in these two experiments ($3.5 \times 10^{14} \text{ W cm}^{-2}$). Thus, the difference in excitation and ablation conditions of the Se target led to a crucial modification of the harmonics distribution, resulting in efficient and non-efficient demonstration of the RH effect using different fluencies of the heating picosecond pulses on the target surface.

The plasmas produced by the laser ablation of the Se bulk target at high fluencies may contain a relatively large number of free electrons. The meaning of a “large number of free electrons” should be clarified from the point of view of their concentration compared with the concentration of the atoms and ions in the Se plasma. All studies of HHG in laser-induced plasmas since 2005, when the optimal conditions of the plasma formation were demonstrated for the first time [44], were carried out under conditions of so-called low-dense plasma ($\leq 5 \times 10^{17} \text{ cm}^{-3}$). Denser laser-induced plasmas, though increasing the number of harmonics emitters, cause the appearance of a large number of free electrons, leading to the destruction of the phase-matching conditions. Correspondingly, efforts were made to maintain a small concentration of electrons, or, in other words, a small ionization rate of plasma during laser ablation. The methods for determination of the neutrals, ions, and electron densities in such plasmas were calculated using different codes.

The medium used for HHG in present studies is low-density plasma. The density of plasma estimated and calculated by different means (thermodynamic code HYADES and molecular dynamics code ITAP IMD) at the used fluencies of heating pulses does not exceed $5 \times 10^{17} \text{ cm}^{-3}$. The corresponding ionization rates, which differ from each other for achieving the “optimal” plasmas using different targets, are found to be between 5 and 10%. Correspondingly, the electron densities do not exceed $5 \times 10^{16} \text{ cm}^{-3}$. Experience shows that, at this concentration, the influence of free electrons on the process of efficient HHG in such plasmas is insignificant.

At these small densities of plasma, the collision and relaxation processes, which affect the concentration and temperature of the plasma at high densities, do not play an important role. Correspondingly, the processes of relaxation and collision do not influence the phase matching of the harmonics since the concentration of plasma does not change between the beginning of plasma formation and the arrival of the densest part of plasma cloud in the area of the driving pulse propagation.

The HHG in other atomic and molecular plasmas was compared in [45]. The referenced paper [45] analyzed modification of the RH (H9) at the beginning of the plateau generated in zinc plasma, contrary to the present case demonstrating and analyzing the RH (H35) lying quite far from the H9. This is a significant difference between the referenced and present studies. Another difference is the usefulness of the RH in different spectral ranges demonstrated in these two studies. RH in the case of Zn plasma enhances the generation in the 89.6 nm region of XUV ($E_{\text{ph}} = 15.4 \text{ eV}$), where other neighboring harmonics from many plasmas have also strong intensity. Contrary to that, the present study provides a detailed analysis of Se-containing plasmas for the optimization of RH in the region where the photon energy ($E_{\text{ph}} = 54 \text{ eV}$) is almost four times larger, which is a notable advantage, taking into account the complexity of achieving the proper phase-matching conditions in the shorter-wavelength region of XUV. Finally, the difference in the applications of these two studies of the molecular plasma comprising ZnSe is underlined by the analysis of the influence of this molecule on the RH effect in different spectral ranges attributed to the RHs in Zn (89.6 nm) and Se (22.9 nm). The common thing here is the conclusion taken from the two studies, i.e., the disappearance of the RH effect due to the influence of the second atom in a molecular compound on the spectral properties of the atom under investigation. In the present paper, this assumption was confirmed in two sets of experiments using ZnSe and HgSe molecular plasmas. Finally, the disappearance of RH effect in two studies was observed under different experimental conditions (delay, pulse duration of heating radiation, fluence of pulses, etc.), as well as different spectral ranges.

In the referenced paper [45] describing studies of Zn and, particularly, ZnSe plasmas for the analysis of resonance effect, only the longer-wavelength range of XUV (50–120 nm) was presented due to the main topic of those studies (RH in the range of 90 nm). In the

present paper, the studies were concentrated on the shorter wavelength region of harmonics distribution from the ZnSe plasma (down to 20 nm, Figure 3b). Nevertheless, the latter spectrum contains the region of 90 nm where the 9th harmonic generates. It is seen that this harmonic does not show any enhancement, thus supporting the previous conclusion about the distraction of the RH effect in this plasma. The present study shows much better conditions for harmonics generation in ZnSe plasma with regard to the results presented in [45] (compare the extension of harmonics up to the 35th order in this manuscript and the generation of the barely seen 17th harmonic in the referenced article). However, even under these favorable conditions, neither H9 nor H35 was enhanced. A similar conclusion was reported in [46].

The physical mechanisms leading to the same effect (i.e., destruction of the RH process) in the vicinity of the RHs in the case of Zn and Se may differ from each other. Correspondingly, they can differently affect the RHs in the cases of Se- and Zn-containing molecular plasmas. One can consider a destructive interference mechanism, as well as a detuning or shifting of the resonant transition, which reduces the gf of this transition, as the mechanisms differently affecting the lower- and higher-order harmonic spectra in the case of Se- and Zn-containing molecular plasmas. Hence, the decreased resonant harmonic yield in the studied case might be due to the modification of the position of the resonant transition of Se influenced by the Hg and Zn components. This influence of the molecular components may diminish the gf of the transition, thus leading to the decay in the enhancement of single harmonic. Meanwhile, in the case of Zn, the role of the above processes can be diminished or exaggerated. Apart from the above assumptions, the consideration of the physics of RH should be taken into account, which may be different for the Se and Zn cases.

4. Conclusions

The high-order harmonics generation in Se-containing laser-induced plasmas was reported. The enhanced 35th harmonic was observed and analyzed using different methods of plasma formation by nanosecond, picosecond, and femtosecond pulses. The enhancement factor of the resonance harmonic was measured to be 32 compared with the neighboring lower-order harmonics. The influence of the compounds of Se-containing species on the diminishing of the resonance effect was analyzed. It was shown that the molecular (ZnSe and HgSe) species suppress the generation of an enhanced 35th harmonic. The reasons for the suppression of this harmonic in the case of Se-containing molecular plasmas were discussed. The same feature was observed in the case of the two-color pump of Se plasma. The involvement of doubly charged ions in the extension of the harmonic cutoff was suggested.

Funding: European Regional Development Fund (1.1.1.5/19/A/003), World Bank Project (REP-04032022-206).

Institutional Review Board Statement: Not applicable.

Informed Consent Statement: Not applicable.

Data Availability Statement: Data underlying the results presented in this paper is not publicly available at this time but may be obtained from the author upon reasonable request.

Acknowledgments: R.A.G. thanks H. Kuroda for providing access to the laser facility and acknowledges the help of V. V. Kim during the characterization of Se plasma.

Conflicts of Interest: The author declares no conflict of interest.

References

1. Ganeev, R.A.; Suzuki, M.; Baba, M.; Kuroda, H. Generation of strong coherent extreme ultraviolet radiation from the laser plasma produced on the surface of solid targets. *Appl. Phys. B* **2005**, *81*, 1081–1089. [[CrossRef](#)]
2. Ganeev, R.A.; Suzuki, M.; Baba, M.; Kuroda, H.; Ozaki, T. Strong resonance enhancement of a single harmonic generated in extreme ultraviolet range. *Opt. Lett.* **2006**, *31*, 1699–1701. [[CrossRef](#)]
3. Ozaki, T.; Bom, L.B.E.; Ganeev, R.; Kieffer, J.-C.; Suzuki, M.; Kuroda, H. Intense harmonic generation from silver ablation. *Laser Part. Beams* **2009**, *25*, 321–325. [[CrossRef](#)]

4. Singhal, H.; Ganeev, R.A.; Naik, P.A.; Srivastava, A.K.; Singh, A.; Chari, R.; Khan, R.A.; Chakera, J.A.; Gupta, P.D. Study of high-order harmonic generation from nanoparticles. *J. Phys. B* **2010**, *43*, 025603. [[CrossRef](#)]
5. Elouga Bom, L.B.; Haessler, S.; Gobert, O.; Perdrix, M.; Lepetit, F.; Hergott, J.-F.; Carré, B.; Ozaki, T.; Salières, P. Attosecond emission from chromium plasma. *Opt. Express* **2011**, *19*, 3677–3683. [[CrossRef](#)] [[PubMed](#)]
6. Ganeev, R.A.; Hutchison, C.; Zaïr, A.; Witting, T.; Frank, F.; Okell, W.A.; Tisch, J.W.G.; Marangos, J.P. Enhancement of high harmonics from plasmas using two-color pump and chirp variation of 1 kHz Ti: Sapphire laser pulses. *Opt. Express* **2012**, *20*, 90–100. [[CrossRef](#)] [[PubMed](#)]
7. Haessler, S.; Strelkov, V.V.; Elouga Bom, L.B.; Khokhlova, M.; Gobert, O.; Hergott, J.-F.; Lepetit, F.; Perdrix, M.; Ozaki, T.; Salières, P. Phase distortions of attosecond pulses produced by resonance-enhanced high harmonic generation. *New J. Phys.* **2013**, *15*, 013051. [[CrossRef](#)]
8. Ganeev, R.A.; Toşa, V.; Kovács, K.; Suzuki, M.; Yoneya, S.; Kuroda, H. Influence of ablated and tunneled electrons on quasi-phase-matched high-order-harmonic generation in laser-produced plasma. *Phys. Rev. A* **2015**, *91*, 043823. [[CrossRef](#)]
9. Rosenthal, N.; Marcus, G. Discriminating between the role of phase matching and that of the single-atom response in resonance plasma-plume high-order harmonic generation. *Phys. Rev. Lett.* **2015**, *115*, 133901. [[CrossRef](#)]
10. Ganeev, R.A.; Suzuki, M.; Yoneya, S.; Kuroda, H. Resonance-enhanced harmonic generation in nanoparticle-containing plasmas. *J. Phys. B* **2015**, *48*, 165401. [[CrossRef](#)]
11. Wostmann, M.; Splittthoff, L.; Zacharias, H. Control of quasi-phase-matching of high-harmonics in a spatially structured plasma. *Opt. Express* **2018**, *26*, 14524–14537. [[CrossRef](#)]
12. Liang, J.; Lai, Y.H.; Fu, W.; Shan, Y.; Yu, W.; Guo, C. Observation of resonance-enhanced high-order harmonics from direct excitation of metal nanoparticles with femtosecond pulses. *Phys. Rev. A* **2020**, *102*, 053117. [[CrossRef](#)]
13. Ganeev, R.A.; Kuroda, H. Resonance-affected high-order harmonic emission from atomic and molecular chromium laser-induced plasmas. *OSA Contin.* **2021**, *4*, 1545–1554. [[CrossRef](#)]
14. Ganeev, R.A. Influence of micro- and macro-processes on the high-order harmonic generation in laser-produced plasma. *J. Appl. Phys.* **2016**, *119*, 113104. [[CrossRef](#)]
15. Ganeev, R.A.; Suzuki, M.; Baba, M.; Kuroda, H. Harmonic generation in XUV from chromium plasma. *Appl. Phys. Lett.* **2005**, *86*, 131116. [[CrossRef](#)]
16. Ganeev, R.A.; Witting, T.; Hutchison, C.; Frank, F.; Tudorovskaya, M.; Lein, M.; Okell, W.A.; Zaïr, A.; Marangos, J.P.; Tisch, J.W.G. Isolated sub-fs XUV pulse generation in Mn plasma ablation. *Opt. Express* **2012**, *20*, 25239–25248. [[CrossRef](#)]
17. Ganeev, R.A.; Suzuki, M.; Yoneya, S.; Kuroda, H. High-order harmonic generation during propagation of femtosecond pulses through the laser-produced plasmas of semiconductors. *J. Appl. Phys.* **2015**, *117*, 023114. [[CrossRef](#)]
18. Fareed, M.A.; Strelkov, V.V.; Singh, M.; Thire, N.; Mondal, S.; Schmidt, B.E.; Legare, F.; Ozaki, T. Harmonic generation from neutral manganese atoms in the vicinity of the giant autoionization resonance. *Phys. Rev. Lett.* **2018**, *121*, 023201. [[CrossRef](#)]
19. Boltaev, G.S.; Ganeev, R.A.; Shuklov, I.A.; Lizunova, A.A.; Dyomkin, D.V.; Milenkovich, T.; Abu Baker, A.; Alnaser, A.S. Studies of the low- and high-order optical nonlinearities of mercury selenide quantum dots using femtosecond pulses. *Appl. Phys. B* **2023**, *129*, 100. [[CrossRef](#)]
20. Kim, V.V.; Grube, J.; Butikova, J.; Sarakovskis, A.; Ganeev, R.A. Influence of chromium plasma characteristics on high-order harmonics generation. *Appl. Phys. B* **2022**, *128*, 217. [[CrossRef](#)]
21. Quintana, M.; Haro-Poniatowski, E.; Morales, J.; Batina, N. Synthesis of selenium nanoparticles by pulsed laser ablation. *Appl. Surf. Sci.* **2002**, *195*, 175–186. [[CrossRef](#)]
22. Oujja, M.; Lopez-Quintas, I.; Benítez-Cañete, A.; de Nalda, R.; Castillejo, M. Harmonic generation by atomic and nanoparticle precursors in a ZnS laser ablation plasma. *Appl. Surf. Sci.* **2017**, *392*, 572–580. [[CrossRef](#)]
23. Corkum, P.B. Plasma perspective on strong-field multiphoton ionization. *Phys. Rev. Lett.* **1993**, *71*, 1994–1997. [[CrossRef](#)] [[PubMed](#)]
24. Tate, J.; Auguste, T.; Muller, H.G.; Salières, P.; Agostini, P.; DiMauro, L.F. Scaling of wave-packet dynamics in an intense midinfrared field. *Phys. Rev. Lett.* **2007**, *98*, 013901. [[CrossRef](#)]
25. Takahashi, E.; Lan, P.; Mucke, O.D.; Nabekawa, Y.; Midorikawa, K. Attosecond nonlinear optics using gigawatt-scale isolated attosecond pulses. *Nat. Commun.* **2013**, *4*, 2691. [[CrossRef](#)] [[PubMed](#)]
26. Strelkov, V. Role of autoionizing state in resonant high-order harmonic generation and attosecond pulse production. *Phys. Rev. Lett.* **2010**, *104*, 123901. [[CrossRef](#)]
27. Milošević, D.B. High-energy stimulated emission from plasma ablation pumped by resonant high-order harmonic generation. *J. Phys. B* **2007**, *40*, 3367. [[CrossRef](#)]
28. Milošević, D.B. Resonant high-order harmonic generation from plasma ablation: Laser intensity dependence of the harmonic intensity and phase. *Phys. Rev. A* **2010**, *81*, 023802. [[CrossRef](#)]
29. Tudorovskaya, M.; Lein, M. High-order harmonic generation in the presence of resonance. *Phys. Rev. A* **2011**, *84*, 013430. [[CrossRef](#)]
30. Ishikawa, K. Photoemission and ionization of He⁺ under simultaneous irradiation of fundamental laser and high-order harmonic pulses. *Phys. Rev. Lett.* **2003**, *91*, 043002. [[CrossRef](#)]
31. Huo, X.-X.; Wang, S.; Sun, L.; Xing, Y.-H.; Zhang, J.; Liu, X.S. Anomalous resonance-enhanced harmonic ellipticity in an elliptically polarized laser field. *Phys. Rev. A* **2022**, *106*, 023102. [[CrossRef](#)]

32. Lai, Y.H.; Rao, K.S.; Liang, J.; Wang, X.; Guo, C.; Yu, W.; Li, W. Resonance-enhanced high harmonic in metal ions driven by elliptically polarized laser pulses. *Opt. Lett.* **2021**, *46*, 2372–2375. [[CrossRef](#)]
33. Ganeev, R.A. Higher harmonics generation for intense laser radiation in plasma created by a prepulse acting on the surface of a solid target. *Phys. Uspekhi* **2009**, *52*, 55–77. [[CrossRef](#)]
34. Ganeev, R.A. *Resonance Enhancement in Laser-Produced Plasmas: Concepts and Applications*; Wiley: New York, NY, USA, 2018.
35. Ganeev, R.A.; Boltaev, G.S.; Kim, V.V.; Iqbal, M.; Kuroda, H.; Alnaser, A.S. Distinction in resonance properties of the atomic and molecular contained plasmas used for high-order harmonics generation of ultrafast laser pulses. *J. Appl. Phys.* **2021**, *129*, 043103. [[CrossRef](#)]
36. Venkatesh, M.; Kim, V.V.; Boltaev, G.S.; Konda, S.R.; Svedlindh, P.; Li, W.; Ganeev, R.A. High-order harmonics generation in MoS₂ transition metal dichalcogenides: Effect of nickel and carbon nanotube dopants. *Int. J. Mol. Sci.* **2023**, *24*, 6540. [[CrossRef](#)] [[PubMed](#)]
37. Kim, V.V.; Boltaev, G.S.; Iqbal, M.; Abbasi, N.A.; Al-Harmi, H.; Wahyutama, I.S.; Sato, T.; Ishikawa, K.L.; Ganeev, R.A.; Alnaser, A.S. Resonance enhancement of harmonics in the vicinity of 32 nm spectral range during propagation of femtosecond pulses through the molybdenum plasma. *J. Phys. B* **2020**, *53*, 195401. [[CrossRef](#)]
38. Wahyutama, I.S.; Sato, T.; Ishikawa, K.L. Time-dependent multiconfiguration self-consistent-field study on resonantly enhanced high-order harmonic generation from transition-metal elements. *Phys. Rev. A* **2019**, *99*, 063420. [[CrossRef](#)]
39. Rao, K.R.; Murti, S.G.K. Investigations on the spectrum of selenium. IV. Se I and Se VII. *Proc. R. Soc. Lond. A* **1934**, *145*, 694–698.
40. Martin, D.C. Analysis of the spectrum of Se II. *Phys. Rev.* **1935**, *48*, 938–944. [[CrossRef](#)]
41. Gibson, S.T.; Greene, J.P.; Rušćić, B.; Berkowitz, J. Photoionisation of atomic selenium. *J. Phys. B* **1986**, *19*, 2841–2848. [[CrossRef](#)]
42. Esteves, D.A.; Bilodeau, R.C.; Sterling, N.C.; Phaneuf, R.A.; Kilcoyne, A.L.D.; Red, E.C.; Aguilar, A. Absolute high-resolution Se⁺ photoionization cross-section measurements with Rydberg-series analysis. *Phys. Rev. A* **2011**, *84*, 013406. [[CrossRef](#)]
43. Kramida, A.; Ralchenko, Y.; Reader, J.; NIST ASD Team. *NIST Atomic Spectra Database (Version 5.9)*; National Institute of Standards and Technology: Gaithersburg, MD, USA, 2023. Available online: <https://physics.nist.gov/asd> (accessed on 2 May 2023).
44. Ganeev, R.; Suzuki, M.; Baba, M.; Kuroda, H.; Ozaki, T. High-order harmonic generation from boron plasma in the extreme-ultraviolet range. *Opt. Lett.* **2005**, *30*, 768–770. [[CrossRef](#)] [[PubMed](#)]
45. Ganeev, R.A.; Kuroda, H. High-order harmonics generation in atomic and molecular zinc plasmas. *Photonics* **2021**, *8*, 29. [[CrossRef](#)]
46. Boltaev, G.S.; Abu Baker, A.M.; Iqbal, M.; Abbasi, N.; Ganeev, R.A.; Alnaser, A.S. Low-order nonlinearities and high-order harmonics generation in Zn and ZnSe nanoparticles synthesized during femtosecond laser ablation at 50 kHz pulse repetition rate. *J. Opt. Soc. Am. B* **2022**, *39*, 2794–2803. [[CrossRef](#)]

Disclaimer/Publisher's Note: The statements, opinions and data contained in all publications are solely those of the individual author(s) and contributor(s) and not of MDPI and/or the editor(s). MDPI and/or the editor(s) disclaim responsibility for any injury to people or property resulting from any ideas, methods, instructions or products referred to in the content.